Supplementary information – The effect of data quality and model parameters on the quantitative phase analysis of X-ray diffraction data by the Rietveld method

Matthew R. Rowles*

John de Laeter Centre, Curtin University, Perth, WA Australia

SUPPLEMENTARY TABLES AND FIGURES

This section gives supplementary tables and figures to the main paper.

TABLE S1. Data collection conditions for the diffraction patterns of varying intensity.

Nominal maximum intensity	Tube current (mA)		Step size (° 2θ)		Count time per step (s)		Datasets collected	
	1a	1e	1a	1e	1a	1e	1a	1e
100	5		0.004 585		0.01		1	
100	6	10	0.004 585	0.004 578	0.01	0.01	1	2
300	8	10	0.009 171	0.009 155	0.02	0.03	2	1
500	14	10	0.009 171	0.009 155	0.02	0.05	2	1
1000	11	10	0.009 171	0.009 155	0.05	0.10	1	1
3000	11	20	0.009 171	0.009 155	0.15	0.15	1	1
5000	12	20	0.009 171	0.009 155	0.23	0.25	1	1
10 000	24	40	0.009 171	0.009 155	0.23	0.25	1	1
30 000	36	40	0.009 171	0.009 155	0.46	0.75	1	1
50 000	40	40	0.009 171	0.009 155	0.69	1.25	1	1
100 000	40	40	0.009 171	0.009 155	1.38	2.50	9	9

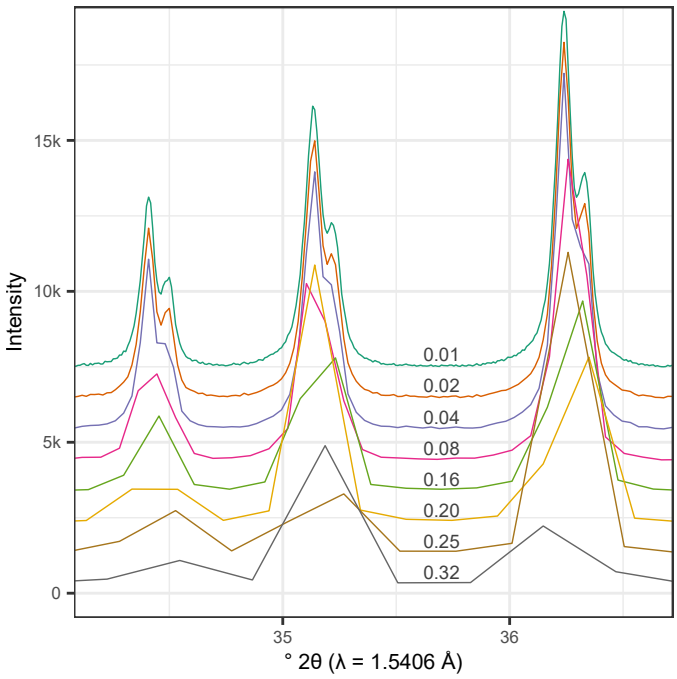

FIG. S1. Diffraction data of sample 1e for all step sizes with a nominal maximum intensity of 20 000 counts. To give diffraction patterns with different step sizes, points were dropped from the original measured data. The patterns are displaced vertically for clarity.

TABLE S2. Nominal and actual (a) step sizes (° 2θ) and (b) maximum intensities (counts) of the diffraction patterns used in the modelling. Every n^{th} datapoint was kept to construct each of the diffraction patterns.

(a)

n	Nominal	1a	1e
1	0.01	0.009 171	0.009 155
2	0.02	0.018 34	0.018 31
4	0.04	0.036 68	0.036 62
9	0.08	0.082 54	0.082 39
17	0.16	0.1559	0.1556
22	0.20	0.2018	0.2014
27	0.25	0.2476	0.2472
35	0.32	0.3210	0.3204

(b)

Nominal	1a	1e	Nominal	1a	1e
100	100	97	20 000	17 200	19 100
200	176	192	50 000	42 900	48 000
500	421	458	100 000	85 900	96 700
1000	826	921	200 000	172 000	195 000
2000	1660	1850	500 000	431 000	488 000
5000	4140	4680	1 000 000	862 000	978 000
10 000	8400	9460			

REFINING A ZERO ERROR

Here are figures and tables derived from the models with a refining zero error in conjunction with a specimen displacement. All other information about the models, data, refinement methods, etc, is as given in the main paper.

TABLE S3. Parameter values used when, according to the refinement type, a given parameter was fixed.

Parameter			Value
Packing density			0.172
Crystallite size Lorentzian (nm)	Cor		313
	Flu		590
	Zin		293
Microstrain Lorentzian	Cor		0.0195
	Flu		0.0415
Unit cell parameter (Å)	Cor	a	4.759 53
		c	12.993 28
	Flu	a	5.464 63
	Zin	a	3.250 05
		c	5.206 97
Isotropic atomic displacement parameter ($Å^2$)	Cor	Al	0.249
		O	0.193
	Flu	Ca	0.468
		F	0.692
	Zin	Zn	0.524
		O	0.321

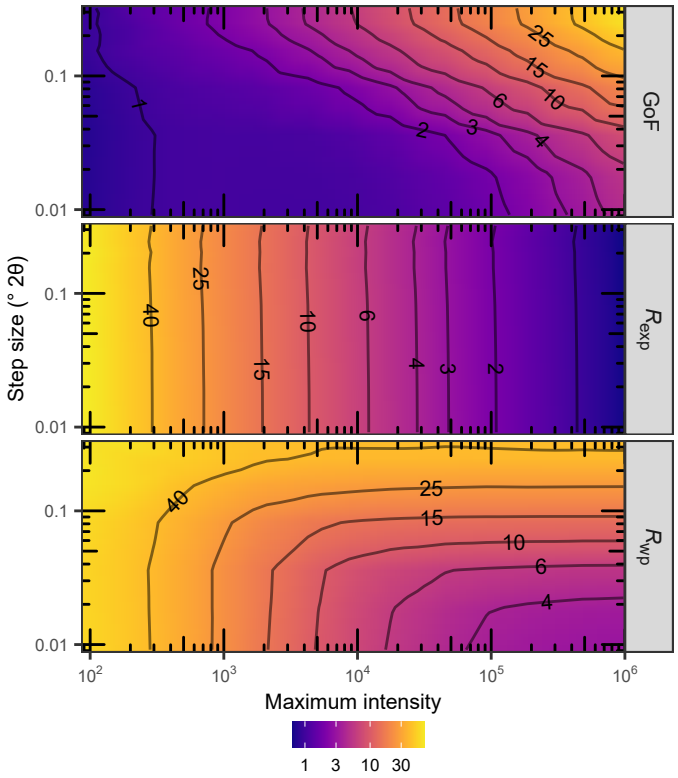

FIG. S2. The figures-of-merit, GoF, R_{exp}, and R_{wp}, for sample 1e/4/150. The trends evident in these plots are repeated throughout all the models. It can be seen that the desire for a low Gof and R_{wp} are at odds with each other with respect to maximum intensity.

* matthew.rowles@curtin.edu.au

[1] H. Toraya, Estimation of statistical uncertainties in quantitative phase analysis using the Rietveld method and the whole-powder-pattern decomposition method, J. Appl. Crystallogr. **33**, 1324 (2000).

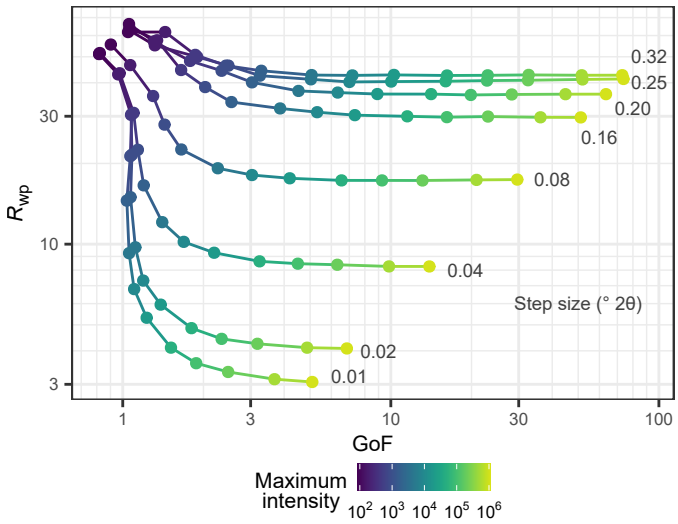

FIG. S3. Comparison of R_{wp} and GoF for all sample 1e averaged over all refinement types and HALs, showing that step size is the best predictor low R_{wp} and GoF, when coupled with a maximum intensity of $\sim 20-50\,000$ counts.

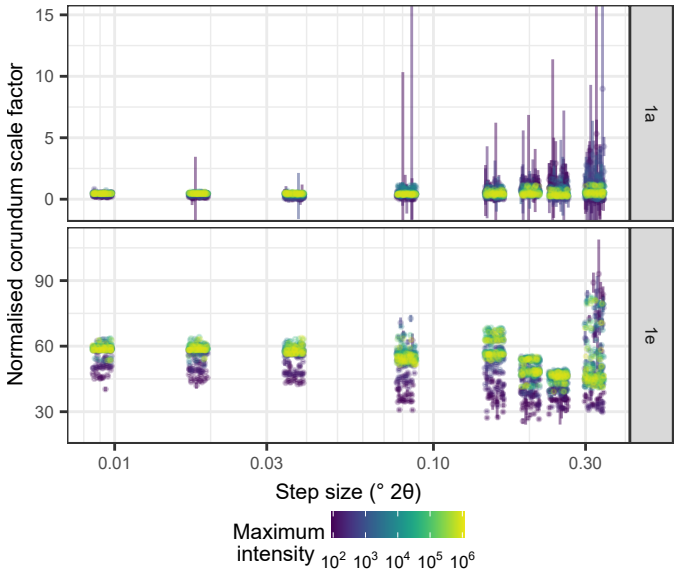

FIG. S4. Scale factors for corundum normalised by maximum intensity for samples 1a and 1e. The error bars represent twice the standard uncertainty. The datapoints have been displaced slightly from their x-axis values for clarity.

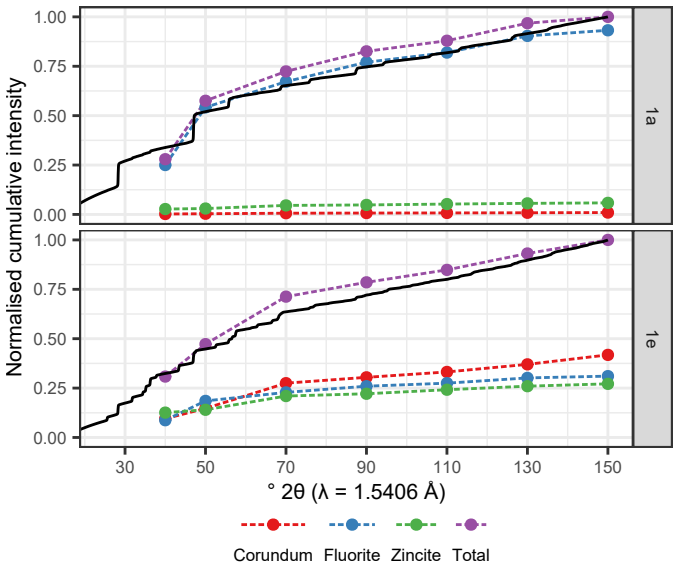

FIG. S5. The cumulative intensity of the diffraction data presented in Figure 1 and the numerical area of the individual phases and their sum normalised to the total diffracted intensity. In both samples 1a and 1e, it can be seen that intensities after 70° 2θ are evenly distibuted. The areas attributed to each phase change in relative distribution with low HAL values for both samples; after the intensities stabilise at 70° 2θ, their relative contributions remain constant.

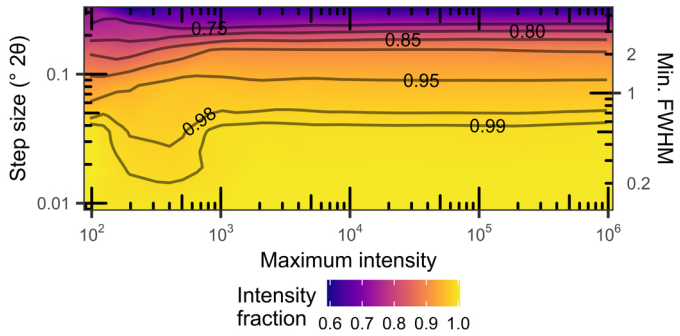

FIG. S6. Fraction of total intensity in sample 1e/3/150 as a ratio of the total intensity present in the 0.01° 2θ step size pattern. The right axis gives the step size as a function of the average FWHM of the first peak, as given in Figure 8.

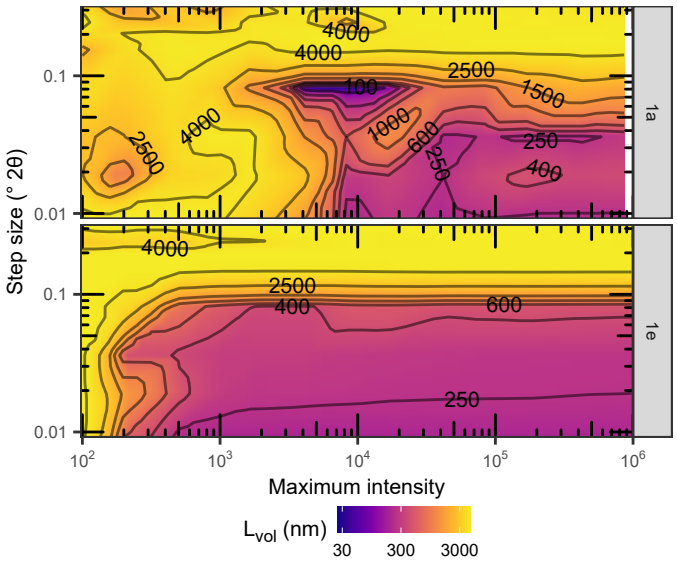

FIG. S7. Crystallite size for corundum in sample 3/150. It can be seen that they only agree for small step sizes and large maximum intensities, due to the ability to properly resolve the requisite peaks.

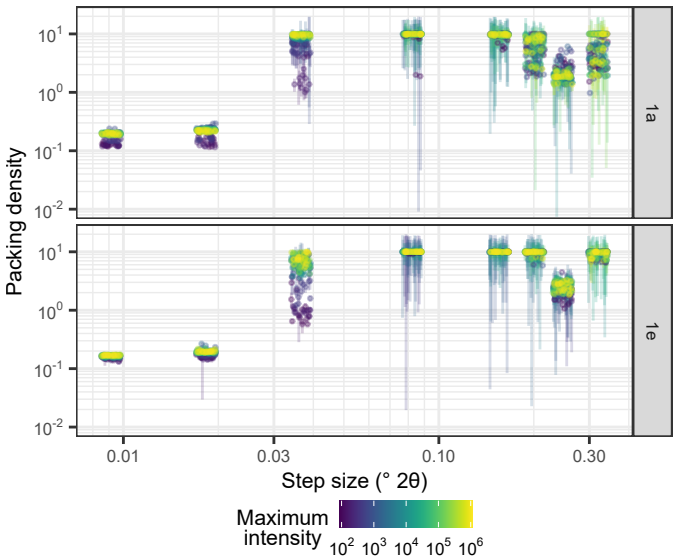

FIG. S8. Packing density for samples 1a and 1e for all intensities and HALs for refinement types 3 and 4. Error bars represent twice the standard uncertainty. The datapoints have been displaced slightly from their x-axis values for clarity.

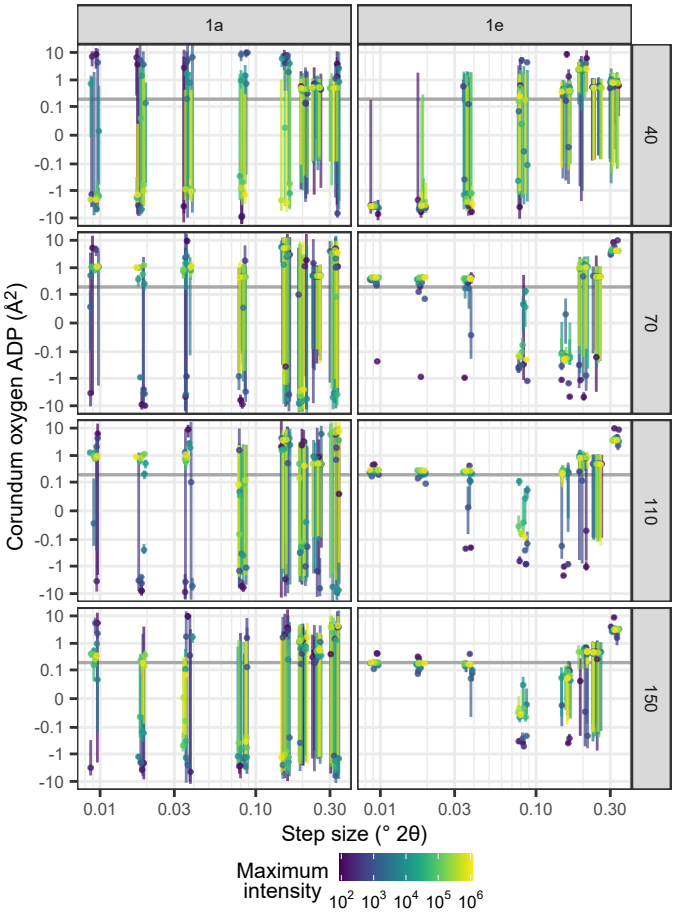

FIG. S9. ADP estimates for oxygen in corundum for for samples 1a and 1e, refinement type 4, and the given HALs. The horizontal gray line represents the value given in Table 3. The error bars represent twice the standard deviation. The standard uncertainty is only of significance for low intensity, small HAL, large stepsize patterns. Please note that the vertial axis is logarithmic. The datapoints have been displaced slightly from their x-axis values for clarity.

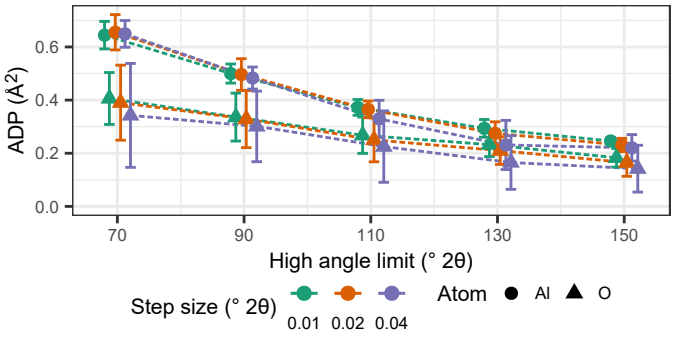

FIG. S10. ADPs for corundum in samples 1e/> 1000. Error bars represent twice the standard deviation of estimates averaged over all intensities. The datapoints have been displaced slightly from their x-axis values for clarity.

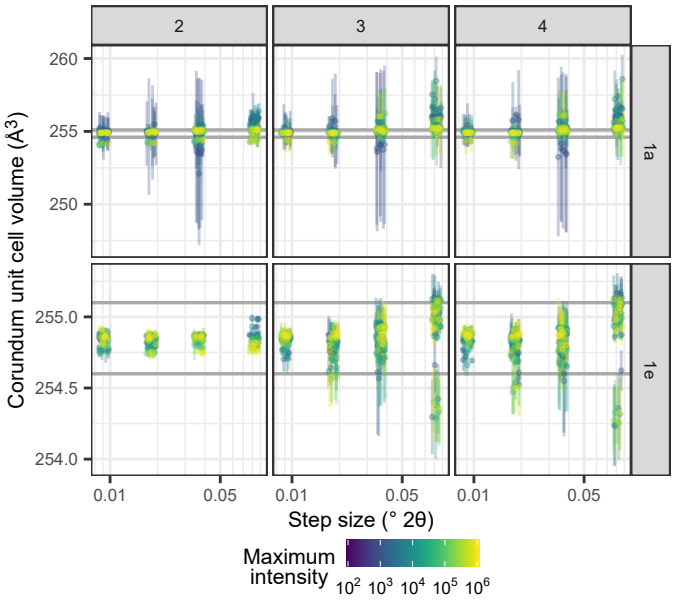

FIG. S11. Spread of calculated unit cell volume for corundum in by refinement type for samples 1a and 1e for all intensities > 500 and all HALs. Error bars represent twice the standard deviation of the estimates. Please note that the vertical axis in the two rows are different; guidelines have been drawn in both rows to indicate an identical vertical range in both rows. The datapoints have been displaced slightly from their x-axis values for clarity.

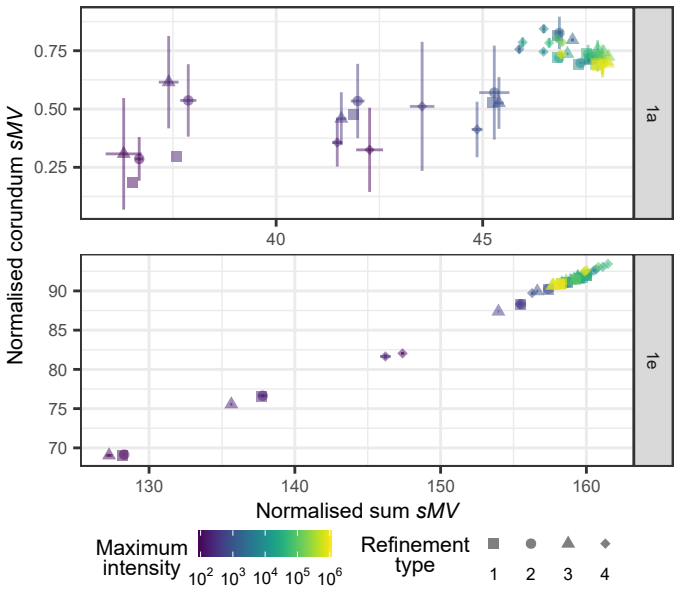

FIG. S12. Comparison of the sMVs for corundum and sum for samples 0.02/110, normalised by maximum intensity. Similar behaviour is exhibited for all refinements. The error bars represent twice the standard deviation.

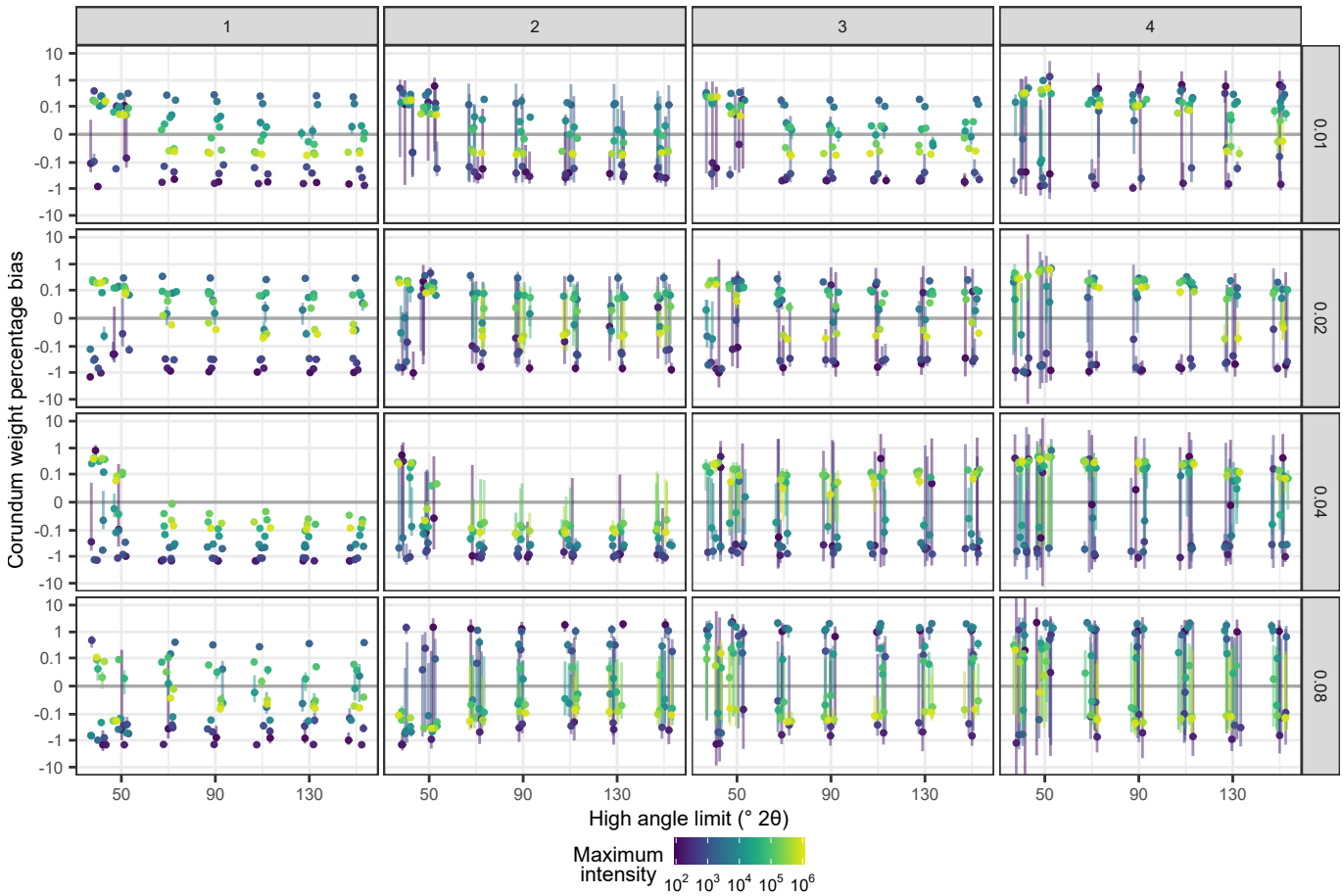

FIG. S13. Absolute corundum weight percentage bias in sample 1a separated by refinement type and stepsize. Error bars represent twice the combined standard deviation and uncertainty. Please note that the vertical axis is logarithmic. For step sizes $> 0.08°$ 2θ, the bias is similar to that of $0.08°$ 2θ, increasing to $\sim 20-50$ percentage points for $0.32°$ 2θ. The datapoints have been displaced slightly from their x-axis values for clarity.

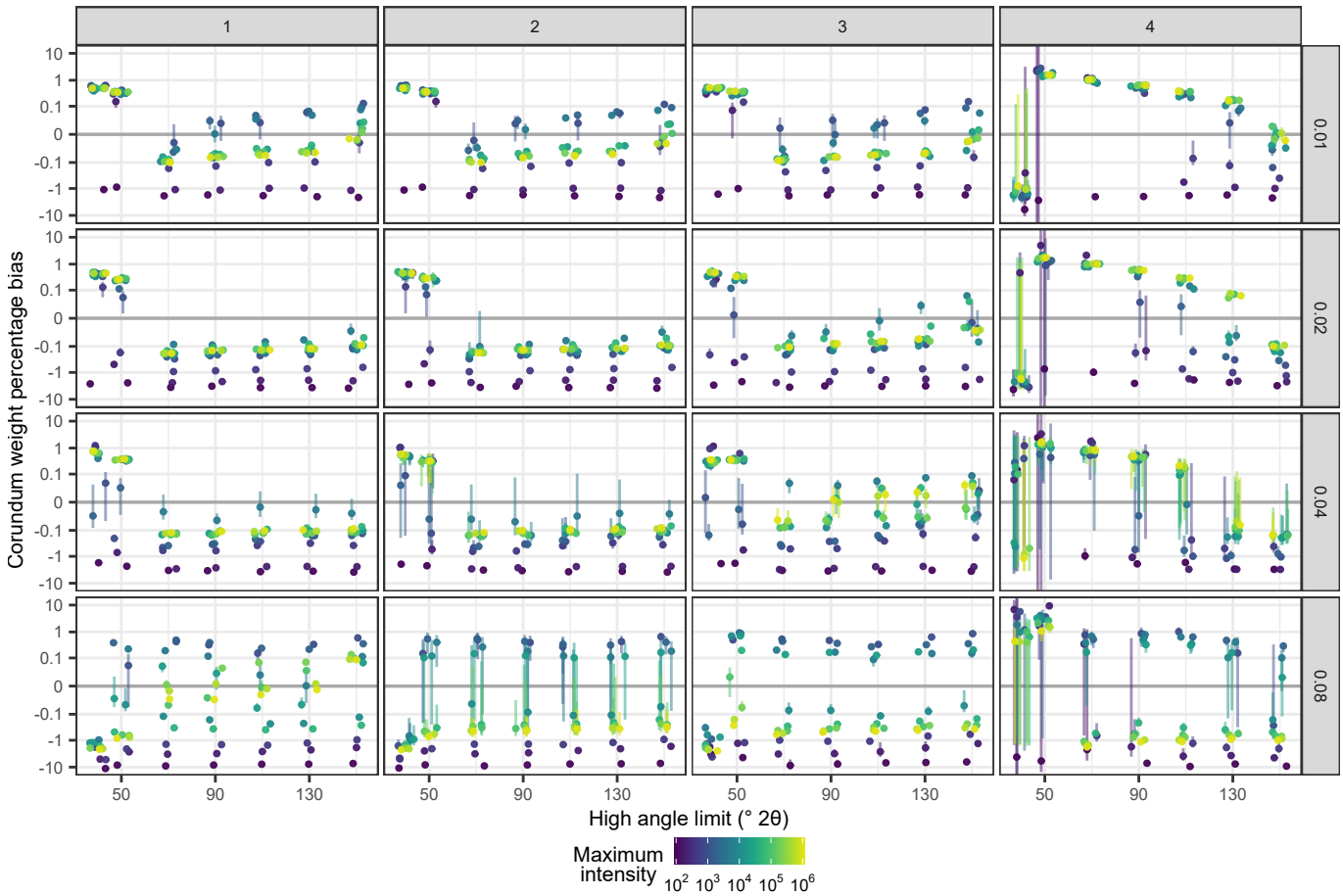

FIG. S14. Absolute corundum weight percentage bias in sample 1e separated by refinement type and stepsize. Error bars represent twice the combined standard deviation and uncertainty. Please note that the vertical axis is logarithmic. For step sizes $> 0.08°$ 2θ, the bias is similar to that of $0.08°$ 2θ, increasing to $\sim$ 20 percentage points for $0.32°$ 2θ. The datapoints have been displaced slightly from their x-axis values for clarity.

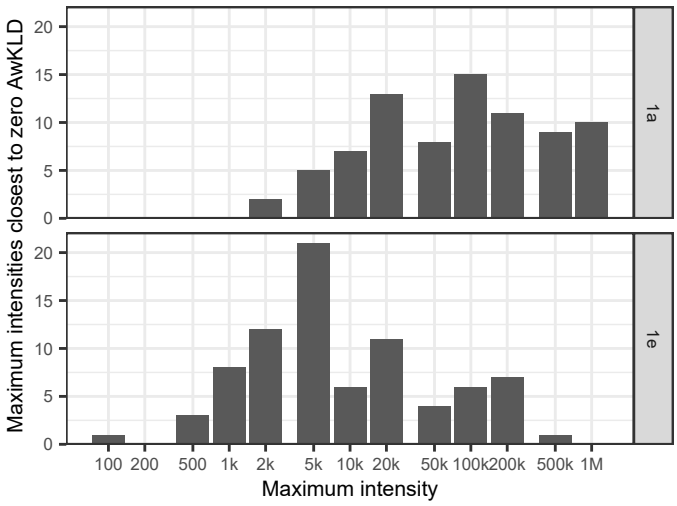

FIG. S15. Histograms showing the number of diffraction patterns for which that particular maximum intensity had the AwKLD value closest to zero, for samples 1a and 1e. The count is taken over samples $\geq 70/\leq 0.08$. It can clearly be seen that the sample with phases present in smaller amounts requires maximum intensities much greater than the sample with phases present at approximately equal amounts.

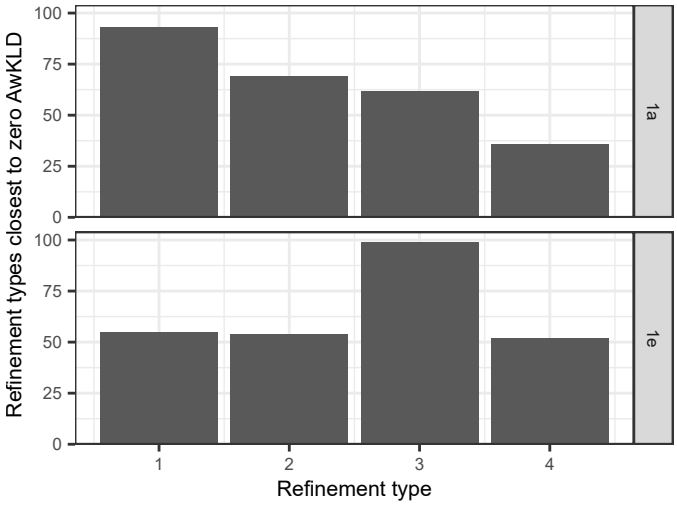

FIG. S16. Histograms showing the number of diffraction patterns for which that refinement type had the AwKLD value closest to zero, for samples 1a and 1e. The count is taken over samples $\geq 70/\leq 0.08$. It can clearly be seen that the sample with phases present in smaller amounts requires a more constrained refinement than the sample with phases present at approximately equal amounts, where even this benefits from not refining ADPs.

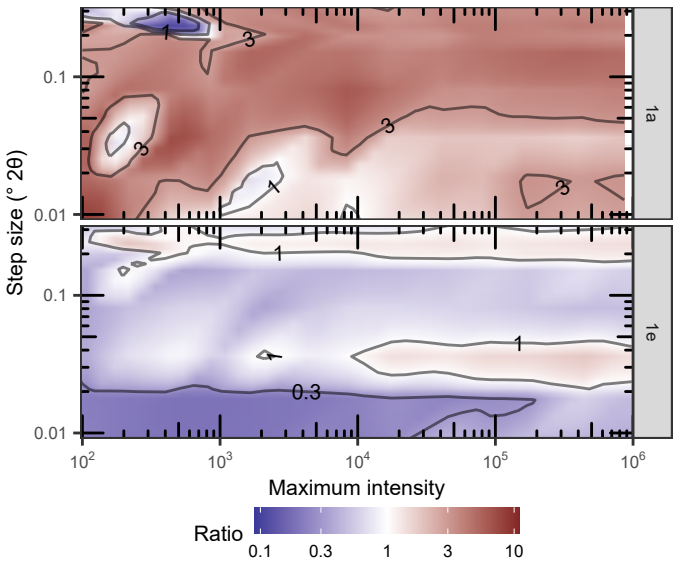

FIG. S17. The ratio, σ_R/σ_T, of the uncertainties of the weight fraction of corundum from sample 4/130 calculated from this study (Eqn 11) and from [1] (Eqn 10), with $D = 1$. It is clear that the Toraya method behaves substantially differently between evenly and unevenly distributed intensities.

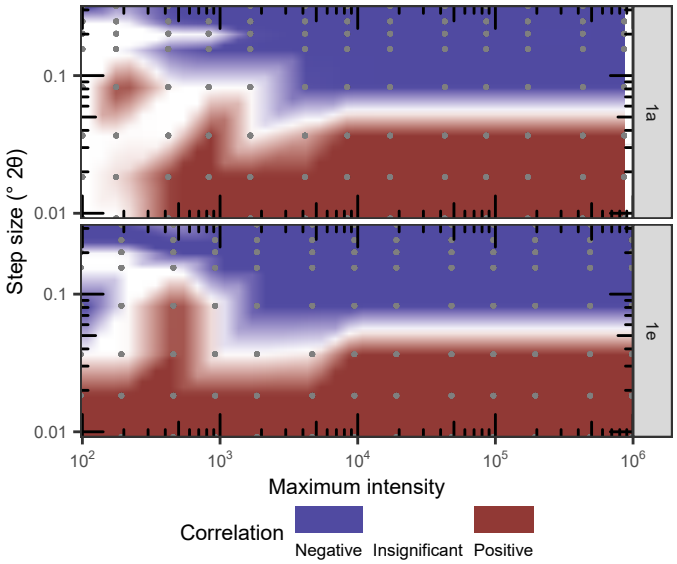

FIG. S18. Regions of negative, insignificant, and positive serial correlation for sample 4/130 according to Eqns 12 – 15. The position of the data making the plot is given by the grey points. The overall behaviour of this plot is the same for all others, with large regions of positive and negative serial correlation present at the bottom and top of the plot, the long white bar moving down slightly, and the large white region becoming a little larger.